

# Adiabatic Pulses

Alberto Tannús<sup>†‡</sup> and Michael Garwood<sup>†</sup>

<sup>†</sup> Center for Magnetic Resonance Research and Department of Radiology, University of Minnesota, Minneapolis, MN 55455, USA

and <sup>‡</sup> Departamento de Física e Informática (DFI-IFSC), Universidade de São Paulo, São Carlos, SP 13560-970, Brazil

Adiabatic pulses are sometimes considered to be mysterious and exotic entities which are difficult to understand, complex to generate and impractical to implement. This work is an attempt to bring familiarity and to fulfill the preliminary needs of anyone interested in learning more about this subject. The response of magnetization to stimuli produced by adiabatic pulses is analyzed using vector representations in a frequency modulated rotating frame. The first section deals with basic principles of amplitude and frequency modulated pulses and a vector representation in a second rotating frame is used to explain how the adiabatic condition can be satisfied. The subsequent section explains the principles of offset independent adiabaticity. These principles are then used to design optimal functions for the amplitude, frequency, and magnetic field gradient modulations for adiabatic inversion pulses. The last section considers some practical aspects for those who want to develop methodologies involving adiabatic pulses. © 1997 John Wiley & Sons, Ltd.

*NMR in Biomed.* 10, 423–434 (1997) No. of Figures: 8 No. of Tables: 2 No. of References: 59

Keywords: radiofrequency pulse; NMR; adiabatic pulse

Received 6 June, 1997; accepted 4 August 1997

## INTRODUCTION

When NMR was first performed,<sup>1,2</sup> resonance was achieved by sweeping the amplitude of the polarizing magnetic field  $B_0$  in the presence of a perpendicular field  $B_1$  which oscillated at a constant radio frequency (RF). This continuous wave (CW) approach has since been replaced by the pulsed NMR experiment<sup>3</sup> which is performed in a static  $B_0$  and uses a pulsed  $B_1$  to excite the full band of spectral frequencies simultaneously. Typically, the carrier frequency of the pulse remains constant and is applied at the center of the spectral region of interest. In this review, we examine an alternative approach in which the carrier frequency varies with time during the pulse. These frequency-swept pulses, known as adiabatic pulses, have benefitted from recent advances which have expanded their capabilities and popularity in applications ranging from *in vivo* imaging to high resolution spectroscopy of isolated molecules. In analogy to the classical CW experiment, the different spectral components are rotated in succession during the adiabatic frequency sweep. When the total sweep time is short relative to  $T_1$ , the transient response of the spin system can be induced, which allows observation of NMR phenomena (e.g. FIDs or echoes) related to the pulsed method. By rapidly sweeping the frequency of the adiabatic pulses, NMR experiments can be performed in the same manner as the pulsed experiment (i.e. the length of adiabatic

pulses can be short enough to permit their use in most pulse sequences). In this manner, the advantages of both classical CW and pulsed NMR approaches can be exploited.

In a sweep of either  $B_0$  (classical experiment) or RF pulse frequency (adiabatic experiment) from one side of resonance to the other, the net rotation of the magnetization vector  $\mathbf{M}$  is highly insensitive to changes in  $B_1$  amplitude. This desirable property has led to the common use of adiabatic pulses in NMR experiments performed with surface coils. Although the  $B_1$  produced by a surface coil varies throughout space, the sensitivity gain provided by such coils is a major advantage for many *in vivo* NMR applications. Within the sensitive volume of a typical surface coil, the amplitude of  $B_1$  varies by >10-fold, which means the flip angle also varies by >10-fold across the sample when conventional (constant frequency) pulses are transmitted with this coil. In many experiments, flip angle errors cause sensitivity losses, quantification errors, and artifacts (e.g. undesirable coherences). Adiabatic pulses offer a means to rotate  $\mathbf{M}$  by a constant flip angle, even when  $B_1$  is extremely inhomogeneous.

Across the spectral bandwidth of interest, spins with different precession frequencies (isochromats) are sequentially rotated as the frequency sweep  $\omega_{\text{RF}}(t)$  approaches the resonance frequency  $\omega_0$  of each isochromat. With some types of adiabatic pulse, such as adiabatic full passage (AFP), the bandwidth  $\Delta\Omega$  is dictated solely by the range of the frequency sweep. For the spins precessing within this frequency band, the flip angle will be uniform, provided that the orientation of the effective magnetic field changes slower than the rotation of  $\mathbf{M}$  about this effective field. This requirement, which is known as the adiabatic condition, can be satisfied by using a sufficiently high  $B_1$  amplitude or by a slow frequency sweep. With the latter method,  $\Delta\Omega$  can be arbitrarily wide, even when using low peak RF power, provided that the pulse length  $T_p$  can be sufficiently long. The ability to achieve uniform flip angles over broad

Contract grant sponsor: NIH

Contract grant number: RR08079

Contract grant number: CA64338

Contract grant sponsor: FAPESP (Brazil)

**Abbreviations used:** AFP, adiabatic full passage; AHP, adiabatic half-passage; AM, amplitude-modulated; BIR,  $B_1$ -insensitive rotation; CW, continuous wave; FM, frequency-modulated; FOCI, frequency offset corrected inversion; GOIA, gradient-modulated offset independent adiabaticity; HS, hyperbolic secant; NOM, numerically optimized modulations; OIA, offset independent adiabaticity; PSD, power spectral density.

bandwidths with low  $B_1$  amplitude is a unique feature of these adiabatic pulses. With conventional constant-frequency pulses,  $\Delta\Omega$  is always inversely proportional to  $T_p$ , whereas  $\Delta\Omega$  and  $T_p$  are independent parameters in certain types of adiabatic pulses. The ability to invert magnetization uniformly across wide bandwidths with arbitrarily low  $B_1$  amplitude has led to a major advance in broadband decoupling with minimal sample heating in high resolution NMR applications.<sup>4-8</sup> With these broadband pulses, *in vivo* NMR can also benefit from reduced peak RF power requirements and the ability to minimize voxel displacement for different chemical shifts.

For almost two decades, major efforts in NMR research have focused on the design of complex RF pulses to compensate for changes in  $B_1$  amplitude and/or to increase bandwidths. A close relative of adiabatic pulses is the composite pulse, which consists of a train of rectangular pulses of different phases.<sup>9,10</sup> Although composite pulses can be derived to compensate for >10-fold variation of  $B_1$  (e.g. see procedure in Ref. 10), adiabatic pulses generally offer the greatest combined immunity to  $B_1$  inhomogeneity and resonance offsets for a given amount of RF power.

In this review, adiabatic pulses will be analyzed theoretically and explored with vector diagrams. Our purpose is to provide an understanding of how magnetization vectors can be rotated by a constant angle, even when  $B_1$  is variable. Pulses to be described include adiabatic half-passage (AHP) and full-passage (AFP), both of which are commonly exploited to generate uniform excitation ( $90^\circ$ ) and inversion ( $180^\circ$ ) in surface coil applications. The discussion will include a relatively new class of composite adiabatic pulses (BIR-1 and BIR-4) which can uniformly rotate magnetization vectors by any desired angle. Also included is an extensive discussion on the design of modulation functions to be used in pulses to allow rotations that are invariant with frequency offsets. A general goal is to provide an understanding of the most common types of adiabatic pulses, with mention of how these pulses can be advantageous in some experimental applications.

## BASIC PRINCIPLES

### Visualizing adiabatic pulses

A classical description of these adiabatic pulses can be understood by considering the components of the magnetic fields and  $\mathbf{M}$  in a reference frame that rotates at the instantaneous frequency  $\omega_{\text{RF}}(t)$ . By convention, this frame is called the frequency-modulated (FM) frame with axis labels  $x'$ ,  $y'$ ,  $z'$ . In the FM frame, the direction of RF field vector  $\mathbf{B}_1(t)$  remains fixed during an adiabatic passage. When the frequency of the pulse deviates from the Larmor frequency  $\omega_0$ , a magnetic field with amplitude equal to  $\Delta\omega/\gamma$  is encountered along the  $z'$ -axis, where  $\Delta\omega = \omega_0 - \omega_{\text{RF}}$ . Figures 1(a) and 1(b) show examples of  $B_1(t)$  and  $\Delta\omega(t)$  modulation functions for adiabatic passages (AHP and AFP).

In the FM frame (Fig. 2(a)), the effective field  $\mathbf{B}_{\text{eff}}(t)$  is the vector sum of the longitudinal field  $\Delta\omega/\gamma$  and  $\mathbf{B}_1(t)$ . In an adiabatic passage,  $\omega_{\text{RF}}$  is time dependent, and therefore  $\mathbf{B}_{\text{eff}}(t)$  changes its orientation at the instantaneous angular velocity,  $d\alpha/dt$ , where

$$\alpha(t) = \arctan \left[ \frac{\gamma B_1(t)}{\Delta\omega(t)} \right] \quad (1)$$

At the beginning of the pulse,  $\omega_{\text{RF}} \ll \omega_0$ , and  $\Delta\omega$  is at its maximum value ( $\Delta\omega_{\text{max}}$ ). Initially  $\Delta\omega/\gamma$  is very large relative to  $B_1$ ; thus, the initial orientation of  $\mathbf{B}_{\text{eff}}$  is approximately collinear with  $z'$ . As  $\omega_{\text{RF}}(t)$  begins to increase,  $\Delta\omega(t)$  decreases and  $\mathbf{B}_{\text{eff}}$  rotates toward the transverse plane. When  $\omega_{\text{RF}}(t) = \omega_0$ ,  $\mathbf{B}_{\text{eff}}$  equals  $\mathbf{B}_1$ . At this point, an AHP ( $90^\circ$  excitation) has been completed. To perform an AFP, the frequency sweep continues past resonance toward  $-\Delta\omega_{\text{max}}$ , leading to a final  $\mathbf{B}_{\text{eff}}$  orientation along  $-z'$ . During the adiabatic passage,  $\mathbf{M}$  follows  $\mathbf{B}_{\text{eff}}(t)$ ,

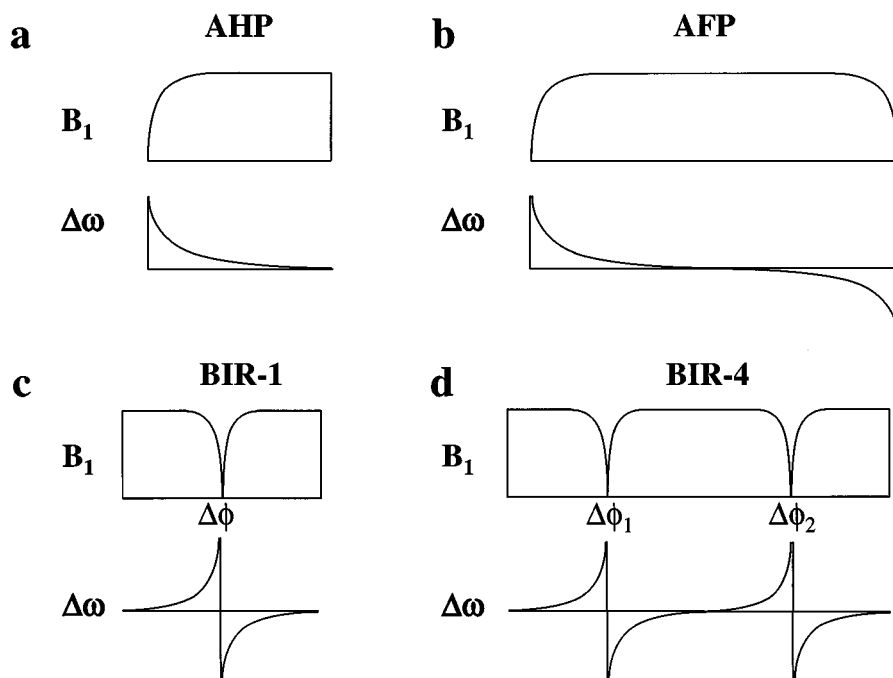
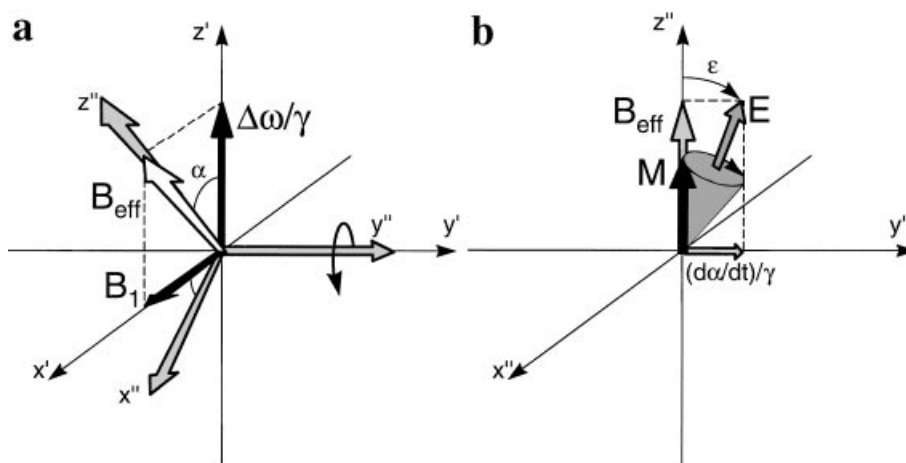


Figure 1. Examples of four adiabatic pulses. Adiabatic passages: (a) AHP and (b) AFP; and  $B_1$ -insensitive rotations, (c) BIR-1 and (d) BIR-4.



**Figure 2.** Vector diagrams showing the effective field and its components in two rotating frames of reference. (a) Relationship between the FM frame,  $x', y', z'$  (thin axes) and the  $B_{\text{eff}}$  frame,  $x'', y'', z''$  (thick axes). (b) Magnetic field components and evolution of the magnetization vector ( $\mathbf{M}$ ) in the  $B_{\text{eff}}$  frame.

provided that the adiabatic condition,  $|\gamma B_{\text{eff}}(t)| \gg |d\alpha/dt|$ , is satisfied for all  $t$ .

#### Vector description of adiabatic passage: FM and $B_{\text{eff}}$ frames

The vector analysis in the FM frame is inadequate to explain why  $\mathbf{M}$  follows  $\mathbf{B}_{\text{eff}}(t)$  during an adiabatic sweep. For this purpose, it is necessary to define a second frame of reference which rotates with  $\mathbf{B}_{\text{eff}}(t)$  called the ' $B_{\text{eff}}$  frame' with axis labels  $x'', y'', z''$ . Figure 2(a) depicts the relationships between the FM and  $B_{\text{eff}}$  frames during an adiabatic passage. Initially, the two frames are superimposable. During the pulse, the  $B_{\text{eff}}$  frame changes its orientation relative to the FM frame at the rate  $d\alpha/dt$ , and  $\mathbf{B}_{\text{eff}}$  remains collinear with the  $z''$ -axis of the  $B_{\text{eff}}$  frame. By the end of the pulse, the two frames are related by an angle which is the net  $\mathbf{B}_{\text{eff}}$  sweep angle (and flip angle). Figure 2(b) shows the relationships between  $\mathbf{M}$  and the magnetic field components in the  $B_{\text{eff}}$  frame. The rotation of the  $B_{\text{eff}}$  frame about the  $y''$ -axis results in a magnetic field with instantaneous magnitude  $(d\alpha/dt)/\gamma$  along the  $y''$ -axis. Thus, in the  $B_{\text{eff}}$  frame, the resultant magnetic field  $\mathbf{E}(t)$  is the vector sum of  $\mathbf{B}_{\text{eff}}(t)$  and  $\gamma^{-1}(d\alpha/dt)\hat{y}''$ . For simplicity, let the  $B_1(t)$  and  $\Delta\omega(t)$  functions be such that  $B_{\text{eff}}$  and  $d\alpha/dt$  are constants. In this case,  $\mathbf{M}$  simply precesses about  $\mathbf{E}$  in the cone of angle  $\varepsilon$ . As shown in Fig. 2(b),  $\mathbf{M}$  never strays beyond an angle  $2\varepsilon$  of  $\mathbf{B}_{\text{eff}}$ , and therefore,  $\mathbf{M}$  also remains within an angle  $2\varepsilon$  of  $\mathbf{B}_{\text{eff}}$  in the FM frame. When the adiabatic condition is well satisfied,  $\varepsilon$  is small and  $\mathbf{E}(t) \approx \mathbf{B}_{\text{eff}}(t)$ . Furthermore, for components of  $\mathbf{M}$  that are initially perpendicular to  $\mathbf{B}_{\text{eff}}(0)$ , the angle between  $\mathbf{B}_{\text{eff}}(t)$  and  $\mathbf{M}$  remains within  $90^\circ \pm \varepsilon$  (i.e.  $\mathbf{M}$  remains approximately perpendicular to  $\mathbf{B}_{\text{eff}}(t)$ ).

The classical adiabatic passage is insensitive to changes in the magnitude of  $\mathbf{B}_1$  only when the net rotation angle is a multiple of  $90^\circ$ , since the final orientation of  $\mathbf{B}_{\text{eff}}$  is insensitive to changes in  $B_1$  amplitude only when the final value of  $|\Delta\omega(t)|$  is zero (e.g. AHP) or is large relative to the final value of  $B_1(t)$  (e.g. AFP). In addition, the adiabatic passages (AHP and AFP) are useful only for rotating a single component of  $\mathbf{M}$  from one point to another and cannot accomplish the 'plane rotations' that many experiments require. For example, to generate optimal spin echo

(SE) signal, the refocusing pulse used in a SE pulse sequence must rotate the components of  $\mathbf{M}$  in the  $x'y'$ -plane about an axis which is invariant to changes in  $\omega_0$  and  $B_1$  amplitude. Although an AFP pulse can sometimes produce an observable echo, such applications generally yield poor results since the phase of the resultant magnetization varies as a function of  $\omega_0$  and  $B_1$  amplitude. Alternatively, as described below, the use of ' $B_{\text{eff}}$  flips' allows the creation of composite adiabatic pulses which can accomplish plane rotation.<sup>11-17</sup> In addition, adjustable phase shifts can be introduced in some of these composite adiabatic pulses to allow the formation of any desired flip angle, while retaining  $B_1$  insensitivity.<sup>14-16, 18</sup> This latter type of pulse is often called a 'universal rotator' since any specified flip angle can be induced for all components of  $\mathbf{M}$  lying perpendicular to a constant rotation axis (i.e. a plane rotation of any desired angle).

#### Adiabatic plane rotation pulses: BIR-1 and BIR-4

Universal rotations can be accomplished with the class of composite adiabatic pulses known as  $B_1$ -insensitive rotation (BIR). BIR pulses (Figs 1(c) and 1(d)) can uniformly rotate all components of magnetization lying in a plane perpendicular to the rotation axis which remains constant despite changes in  $B_1$  amplitude. The first generation plane rotation pulse known as BIR-1 has the disadvantage of producing nonuniform response for Larmor frequencies  $\omega_0$  not equal to the central frequency  $\omega_c$  in the sweep range of  $\omega_{\text{RF}}(t)$ . However, a composite adiabatic pulse known as BIR-4,<sup>14, 15</sup> which consists of double BIR-1, provides a constant rotation axis for moderate resonance offsets ( $|\Omega| = |\omega_0 - \omega_c| > 0$ ). Although BIR-1 does not possess this latter advantage, this pulse is simpler than BIR-4. Thus, we begin with a vector description of BIR-1.

The motions of  $\mathbf{B}_{\text{eff}}$  and  $\mathbf{M}$  during a  $90^\circ$  BIR-1 of length  $T_p$  are shown in Figs 3(a-d). The initial phase of  $\mathbf{B}_1$  is arbitrarily chosen to coincide with  $x'$ . At the beginning of BIR-1,  $\omega_{\text{RF}}$  is applied on resonance ( $\Delta\omega(0)=0$ ). Thus, unlike the classical passage described in the previous section, initially  $\mathbf{B}_{\text{eff}}$  lies in the transverse plane and is perpendicular to  $\mathbf{M}$  (i.e.  $\alpha(0)=90^\circ$ ). A vector analysis similar to that performed in the previous section can be used to prove that the angle between  $\mathbf{B}_{\text{eff}}$  and  $\mathbf{M}$  will remain between  $90^\circ - \varepsilon$  and  $90^\circ + \varepsilon$  during the pulse. To simplify

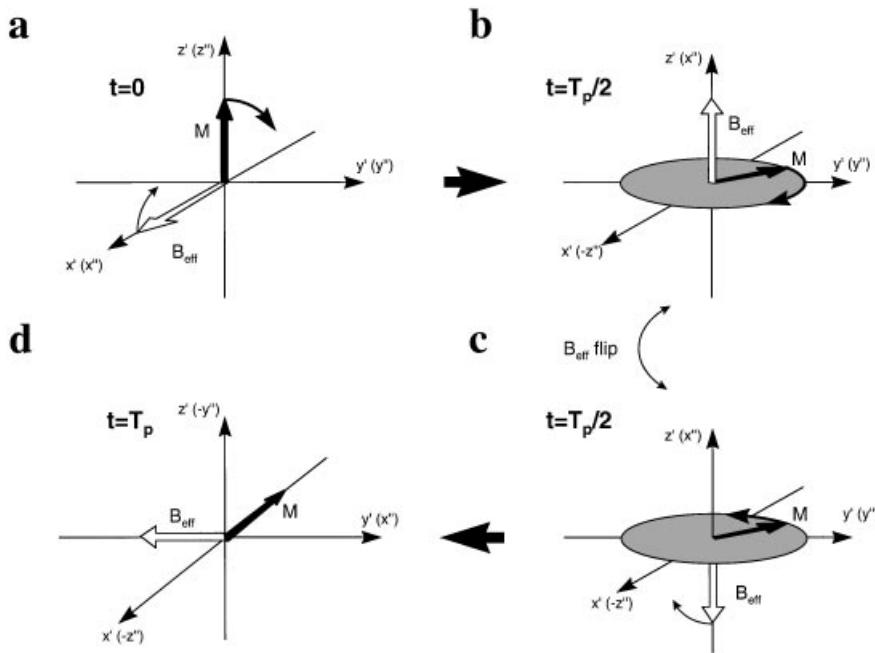


**Figure 3.** (a)–(d) Evolution of  $\mathbf{B}_{\text{eff}}$  and  $\mathbf{M}$  in the FM frame during a  $90^\circ$  BIR-1 (and the first half of a  $180^\circ$  BIR-4). Thick, curved arrows represent precession of  $\mathbf{M}$  around  $\mathbf{B}_{\text{eff}}$ . The evolution of  $\mathbf{B}_{\text{eff}}$  is implied by the thin, curved arrows and the orientation of the  $\mathbf{B}_{\text{eff}}$  frame at each time point ( $t=0$ ,  $T_p/2$  and  $T_p$ ) is indicated by the double primed axes in parentheses.  $\mathbf{B}_{\text{eff}}$  evolves towards  $z'$  (a), while  $\mathbf{M}$  remains perpendicular to it and disperses due to  $B_1$  inhomogeneity (b). At  $t=T_p/2$ ,  $\mathbf{B}_{\text{eff}}$  is instantaneously inverted and the transverse component of  $\mathbf{B}_{\text{eff}}$  (i.e.,  $B_1$ ) is phase shifted by  $270^\circ$  (c). During the second half of BIR-1,  $\mathbf{B}_{\text{eff}}$  evolves towards  $-y'$  and drives  $\mathbf{M}$  back to its initial coherence, which now takes place along  $-x'$  of the FM frame (d). This represents the final state produced by a  $90^\circ$  BIR-1 and the halfway condition for a  $180^\circ$  BIR-4.

the problem, here we assume that the adiabatic condition is well satisfied ( $|\gamma B_{\text{eff}}(t)| \gg |d\alpha/dt|$ ), so that  $\varepsilon$  can be set to zero. During the first half of BIR-1,  $\mathbf{B}_{\text{eff}}$  sweeps from  $x'$  to  $z'$ , while  $\mathbf{M}$  rotates about  $\mathbf{B}_{\text{eff}}$  (Fig. 3(a) and (b)). At  $t=T_p/2$ , the orientation of  $\mathbf{M}$  can be obtained from the solution of the Bloch equation,

$$\frac{d\mathbf{M}}{dt} = [\mathbf{M} \times \gamma \mathbf{B}_{\text{eff}}] = \left[ \mathbf{M} \times \frac{d\psi}{dt} \right] \quad (2)$$

where  $d\psi/dt$  is the rate of change of  $\mathbf{M}$  around  $\mathbf{B}_{\text{eff}}$  since the

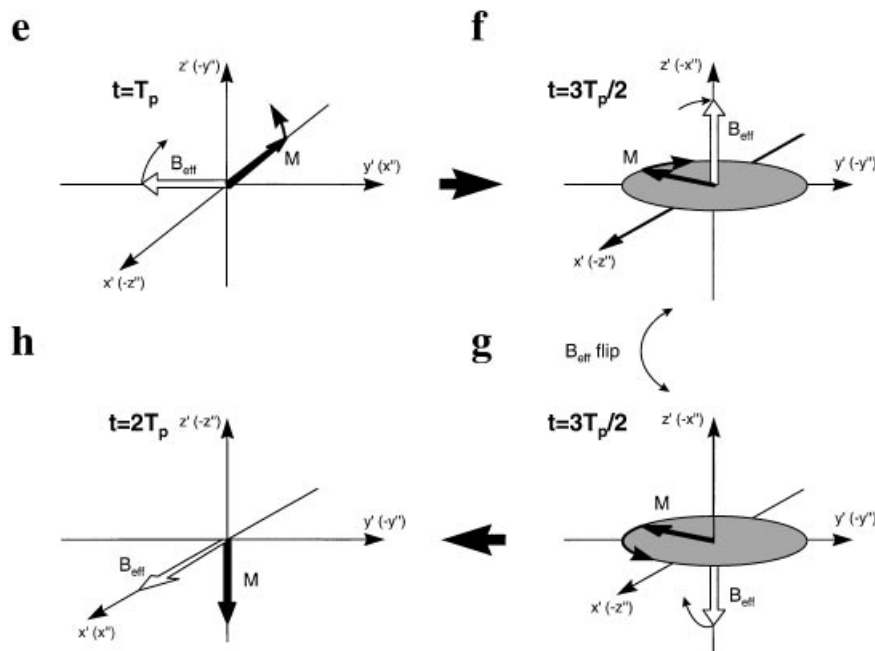


**Figure 3.** (e)–(h) Second half of a  $180^\circ$  BIR-4.  $\mathbf{B}_{\text{eff}}$  continues to evolve from the previous state (d) towards  $z'$  (e). The process of dispersion (f) and coherence recovery (g) repeats with the second  $\mathbf{B}_{\text{eff}}$  flip accompanied by a  $-270^\circ$  phase shift. The final state (h) is achieved with  $\mathbf{B}_{\text{eff}}$  along its initial orientation, but with  $\mathbf{M}$  inverted in the FM frame.

equation has the form of the angular momentum precession equation.<sup>19</sup> Provided that the adiabatic condition was satisfied throughout the first segment of the pulse,  $\mathbf{M}$  is in the  $x'y'$  plane at  $t=T_p/2$  and the accumulated rotation angle ( $\psi$ ) about  $\mathbf{B}_{\text{eff}}$  at this time is simply:

$$\psi(T_p/2) = -\gamma \int_0^{T_p/2} B_{\text{eff}}(t) dt \quad (3)$$

At  $t=T_p/2$ , an instantaneous  $\mathbf{B}_{\text{eff}}$  flip is created by jumping the frequency from  $\Delta\omega_{\text{max}}$  to  $-\Delta\omega_{\text{max}}$  (see BIR-1 in Fig. 1). To produce the desired flip angle  $\theta$ , the phase of  $\mathbf{B}_1$  is simultaneously shifted by  $\Delta\phi=180^\circ+\theta$ . In the present example ( $90^\circ$  BIR-1),  $\Delta\omega=270^\circ$ . During the second half of the pulse (Figs 3(c) and 3(d)),  $\mathbf{B}_{\text{eff}}$  sweeps from  $-z'$  to  $-y'$ , while  $\mathbf{M}$  rotates in the opposite sense about  $x''$ , so that the net  $\psi$  rotation for the pulse is zero. Thus, the central  $B_{\text{eff}}$  flip together with the subsequent time reversal of the modulation functions, compensate (refocus) the  $\psi$  rotations which took place during the first and second halves of the pulse (i.e.  $\psi_{\text{tot}}=0$ ). This phenomenon is equivalent to a rotary echo<sup>20</sup> in the  $B_{\text{eff}}$  frame. The  $\Delta\phi$  phase shift determines the flip angle and the final orientation of the  $B_{\text{eff}}$  frame relative to the FM frame. After this  $90^\circ$  BIR-1, the  $B_{\text{eff}}$  frame is related to the FM frame by a  $-90^\circ$  rotation about  $y'$  and a  $-90^\circ$  rotation about  $x'$ . In the FM frame, the net rotation of  $\mathbf{M}$  is equivalent to a  $90^\circ$  rotation about  $x'$ , followed by a  $90^\circ$  rotation (phase shift) about  $z'$ . It is also possible to show that BIR-1 can induce any flip angle by setting  $\Delta\phi=180^\circ+\theta$ , in which case the net rotation of  $\mathbf{M}$  is equivalent to a  $\theta$  rotation about  $x'$ , followed by a phase shift of  $\theta$ . Although Fig. 3 shows only the motions for a magnetization vector initially oriented along  $z'$ , the plane rotation properties of the pulse can be revealed by performing similar vector analyses using other initial orientations of  $\mathbf{M}$ .

In the presence of a resonance offset  $\Omega$  ( $=\omega_0 - \omega_{\text{RF}}(0) \neq 0$ ), the performance of BIR-1 degrades for two reasons. First, a rotary echo in the  $B_{\text{eff}}$  frame may not be achieved, since  $\psi_{\text{tot}}$  depends on  $B_1(t)$  and  $\omega_0$  according to:

$$\psi_{\text{tot}} = - \int_0^{T_p/2} \sqrt{(\omega_1(t))^2 + (\omega_0 - \omega_{\text{RF}}(t))^2} dt + \int_{T_p/2}^{T_p} \sqrt{(\omega_1(t))^2 + (\omega_0 - \omega_{\text{RF}}(t))^2} dt \quad (4)$$

where  $\omega_1(t) = \gamma B_1(t)$ . When  $\Omega \neq 0$ , the first and second integrals in eq. (4) are unequal, and therefore, the net rotation of  $\mathbf{M}$  about  $\mathbf{B}_{\text{eff}}$  is no longer zero. As described further below, this first problem is eliminated with BIR-4, which is essentially double BIR-1. Secondly, in the presence of a resonance offset, the initial orientation of  $\mathbf{B}_{\text{eff}}$  is no longer perpendicular to  $z'$ , but is given by the angle:

$$\alpha(0) = \arctan \left[ \frac{\omega_1(0)}{(\omega_0 - \omega_{\text{RF}}(0))} \right] \quad (5)$$

As  $|\omega_0 - \omega_{\text{RF}}(0)|$  increases,  $\mathbf{B}_{\text{eff}}(0)$  acquires an increasing longitudinal component in the FM frame, and as a result, an increasing component of the initial longitudinal magnetization is spin locked to  $\mathbf{B}_{\text{eff}}$ . In BIR-4, the component of  $\mathbf{M}$  that becomes spin-locked to  $\mathbf{B}_{\text{eff}}$  is returned to  $z'$  by the end of the pulse, since the initial ( $t=0$ ) and final ( $t=T_p$ ) orientations of  $\mathbf{B}_{\text{eff}}$  are the same. As a consequence, the

desired flip angle is not achieved for an increasing fraction of  $\mathbf{M}$  as frequency offset increases. Like conventional pulses, the only way to alleviate this problem is to increase  $B_1$  amplitude.

The complete sequence of diagrams in Fig. 3 depicts the vector motions of BIR-4. BIR-4 is a composite adiabatic pulse consisting of four segments and two  $\mathbf{B}_{\text{eff}}$  flips, creating a double rotary echo in the  $B_{\text{eff}}$  frame. The third segment begins (Fig. 3(e)) where BIR-1 ends (Fig. 3(d)). BIR-4 uses two phase shifts ( $\Delta\phi_1$  and  $\Delta\phi_2$ ) to produce a flip angle equal to  $\theta$ , where

$$\Delta\phi_1 = 180^\circ + \frac{\theta}{2} \quad (6)$$

$$\Delta\phi_2 = -180^\circ + \frac{\theta}{2} \quad (7)$$

With BIR-4, the  $\theta$  rotation always takes place about an axis which coincides with the initial direction of  $\mathbf{B}_1$  ( $x'$  in the present example). Furthermore,  $\psi_{\text{tot}}$  is always zero following BIR-4, since  $\psi_1 = -\psi_3$  and  $-\psi_2 = \psi_4$  (subscripts denote the  $\psi$  values accumulated in each of the four segments of BIR-4). Of course, satisfactory performance requires that the modulation functions fulfill the adiabatic condition and that  $\omega_0$  is contained in the frequency sweep  $\omega_{\text{RF}}(t)$ .

### Some applications: adiabatic solvent suppression and spectral editing

One of the unique features of BIR-4 (and BIR-1 on resonance) is the fact that the rotation angle is determined simply in the  $\Delta\phi$  phase shifts. These phase shifts can be achieved not only by shifting  $\mathbf{B}_1$  phase, but also by allowing the magnetization vectors to precess in the transverse plane during finite delays inserted in the pulse at the points where  $\Delta\phi_1$  and  $\Delta\phi_2$  normally occur. In the absence of RF irradiation, evolution during each of these delays takes place according to the rotating-frame Hamiltonian describing the spin system. The net transformation achieved by BIR-4 with one or more delays then depends on the combined effects of the  $\Delta\phi$  shifts of  $\mathbf{B}_1$  and the spin evolution that occurred during the delay(s). This general principle forms the basis for a whole series of methods that discriminate based on the spin evolution during the delay(s). These include solvent-suppressive adiabatic pulses,<sup>21-24</sup> adiabatic spectral editing based on spin-spin coupling (BISEP),<sup>25,26</sup> adiabatic multiple quantum coherence filtering,<sup>26,27</sup> and adiabatic polarization transfer.<sup>26,28-30</sup> These pulses and pulse sequences accomplish their tasks while providing a high degree of compensation for  $B_1$  inhomogeneity and are, therefore, particularly advantageous for *in vivo* surface coil studies.

---

## MODULATION FUNCTIONS

---

The recent popularity of adiabatic pulses in MRI and spectroscopy is a predominant factor leading to the rapid progress in the development of these types of pulses. As an example, an analytical solution of the Bloch equations written in the Ricatti form yielded an amplitude and frequency modulated pulse known as the hyperbolic secant

pulse<sup>31,32</sup> (hereafter called HS pulse), which now enjoys wide popularity in high resolution and *in vivo* NMR. The HS pulse is an adiabatic full passage composed of a hyperbolic secant function for amplitude modulation and a hyperbolic tangent function for frequency modulation. An extraordinary property of the HS pulse is its insensitivity to variations of  $B_1$  intensity approaching several orders of magnitude. The desirable plateau of the inversion profile and the sharpness of its transition zones were thought to be unique and curious features of these particular modulation functions. The flat response of the inversion profile was the first known manifestation of offset independent adiabaticity (OIA), although the reason for this was not well understood until recently. In this section we present the theoretical basis for the generation of any pulse shape which can exhibit offset independent adiabaticity, even when the resonance offset is time dependent. A similar development restricted to constant resonance offsets can be found in Refs 33, 34.

Many different functions have been proposed to drive the frequency ( $\Delta\omega(t)$ ) and amplitude ( $\omega_1(t)$ ) modulations of adiabatic pulses.<sup>6, 15, 16, 19, 31, 32, 35–54</sup> Many of these modulation functions were derived from theoretical analyses considering only the isochromat at the center of the excitation band ( $\Omega=0$ ); consequently, the efficiency of these pulses generally degrades as the resonance offset increases except when using the HS pulse.

Modulation functions optimized for specified ranges of  $B_1$  amplitude and/or resonance offset have been derived from considerations of the criterion for adiabaticity.<sup>55</sup> An analytical method, known as NOM,<sup>40, 41</sup> requires a numerical integration which yields the optimal time dependence of the driving functions for  $\Delta\omega(t)$  and  $\omega_1(t)$ . Here we use a similar approach to broaden the bandwidth of AFP pulses while minimizing RF power.

### Offset-independent adiabaticity (OIA)

For the sake of clarity, we first consider offsets,  $\Omega$ , produced for example by a *constant* gradient or chemical shift. Our approach keeps the average RF power constant over the desired bandwidth,  $\Delta\Omega$ . This condition is essential to perform rotations uniformly over a large  $\Delta\Omega$  using either amplitude modulation at a constant pulse frequency or combined amplitude and frequency modulation. Amplitude-modulated (AM) pulses (e.g. sinc pulses) operate by distributing equal amounts of power for every frequency in the bandwidth *at the same time*. In the method used here, the energy is distributed uniformly over the bandwidth, but sequentially in time.<sup>38</sup> This requirement can be fulfilled by adiabatic pulses defined by an AM function:

$$\omega_1(t) = [\omega_0 - \omega_{\text{RF}}(t)]\hat{z}' = \gamma B_1^0 F_1(t)\hat{x} \quad (8)$$

and a frequency-modulated (FM) function;

$$\begin{aligned} \Delta\omega(t) &= [\Omega - AF_2(t)]\hat{z}' \\ &= [\omega_0 - \omega_{\text{RF}}(t)]\hat{z}' \end{aligned} \quad (9)$$

where  $B_1^0$  and  $A$  are the  $B_1(t)$  and frequency sweep amplitudes, respectively, and  $\gamma$  is the gyromagnetic ratio in Hz/Gauss. Equations (8) and (9) describe the components of the effective field experienced by an isochromat with Larmor frequency  $\omega_0$ , in a frame rotating around  $B_0\hat{z}$  with instantaneous frequency  $\omega_{\text{RF}}(t)$  (i.e. the FM frame). As in Ref. 40, we use these equations to express the adiabatic condition as a ratio  $K$ , which here is a function of  $\Omega$  and  $t$ .

For the time interval equal to the pulse duration  $T_p$  and for the offset interval  $|\Omega| \leq A$ ,

$$K(\Omega, t) = \left| \frac{\gamma B_{\text{eff}}^{\Omega}(t)}{\dot{\alpha}} \right| = \frac{A^2 [(\gamma B_1^0 F_1(t)/A)^2 + [F_2(t) - \Omega/A]^2]^{3/2}}{\gamma B_1^0 |(F_2(t) - \Omega/A)F_1(t) - F_1(t)F_2(t)|} \gg 1 \quad (10)$$

where  $B_{\text{eff}}^{\Omega}(t)$  is the effective field as seen by an isochromat at offset frequency  $\Omega$  and  $\dot{\alpha}$  is the rate of change of the  $B_{\text{eff}}^{\Omega}(t)$  orientation expressed in hertz. Our requirement is that the condition stated for  $K(\Omega, t)$  (eq. (10)) must be equally satisfied for all values of  $\Omega$  inside the specified bandwidth. In other words,  $K$  is defined to be constant in  $\Omega$ . It follows that  $K(\Omega, t)$  can be calculated for all specific times  $t = t_{\Omega}$  when the isochromat at  $\Omega$  is on resonance,

$$F_2(t_{\Omega}) = \Omega/A \quad (11)$$

giving;

$$K(t_{\Omega}) = \frac{(\gamma B_1^0 F_1(t_{\Omega}))^2}{AF_2(t_{\Omega})} \gg 1 \quad (12)$$

Hence, the identity;

$$K(t_{\Omega})AF_2(t_{\Omega}) = (\gamma B_1^0 F_1(t_{\Omega}))^2 \quad (13)$$

specifies the relationship between the two driving functions  $F_1(t)$  and  $F_2(t)$ . It states that, for all isochromats with  $|\Omega| \leq A$ ,  $\omega_1(t_{\Omega})^2$  must be much larger than the rate of change of the frequency sweep  $\Delta\omega(t_{\Omega})$  by the same factor  $K(t_{\Omega})$ .

To illustrate the basis of OIA, Fig. 4 shows the field components at three different times during an AFP pulse for the case where  $\Omega \neq 0$ . Far from resonance (Figs 4(a) and 4(c)) the dominant contribution to  $B_{\text{eff}}$  is given by  $\gamma^{-1}\Delta\omega(t) = \gamma^{-1}[\Omega - AF_2(t)]\hat{z}'$ . When resonance is achieved at  $t_{\Omega}$  (Fig. 4(b)), the effective field is solely determined by its transverse component,  $B_1(t_{\Omega})$ ; therefore,  $t_{\Omega}$  is the most critical time in regards to the adiabatic condition. Considering that  $t_{\Omega}$  is a function  $\Omega$ , eq. (13) must be used to calculate modulation functions which yield a constant  $K(t_{\Omega})$  for all isochromats, since it represents the *on-resonance* adiabatic factor for *each one* of them. Any pair of modulation functions that satisfy eq. (13) will achieve uniform adiabaticity as  $AF_2(t)$  sweeps through consecutive values of  $\Omega$ .

Table 1 lists examples of OIA inversion pulses that conform to eq. (13). To compare the performance of the different OIA pulses, some useful parameters were defined.  $B_1^{0(99\%)}$  is the minimum  $B_1$  needed to perform 99% inversion at  $\Omega=0$ .  $B_1^{\text{rms}}$  is the root mean square (rms) value of  $B_1(t)$ . The last column lists the quality factor  $Q = \Delta\Omega_{90\%}/\gamma B_1^{\text{rms}}$ , where  $\Delta\Omega_{90\%}$  is the effective bandwidth for >90% inversion of  $M_z$  (i.e.  $M_z/M_0 < -0.8$ ). All parameters were calculated using  $A = 25$  kHz and  $T_p = 2$  ms. As expected from eq. (13), all pulses listed in Table 1 require approximately the same  $B_1^{\text{rms}}$ . Pulses with the flattest AM functions perform rotations with the lowest  $B_1^{0(99\%)}$  since the RF energy is distributed more evenly in time. The ideal AM shapes approach that of the chirp pulse, but with smooth transitions to zero at the extremities. Similar shapes are predicted when optimizing bandwidth by NOM procedures<sup>1</sup> and by stretching known adiabatic pulses.<sup>49</sup> To approach this condition, we developed a class of flattened HS pulses with driving functions<sup>34</sup> based on a nonlinear argument,  $\eta(\tau) = \beta\tau^p$  ( $\tau = 2t/T_p - 1$ , for  $t$  in the range  $[0, T_p]$ ). With these new pulses, called HS<sub>n</sub> pulses, the

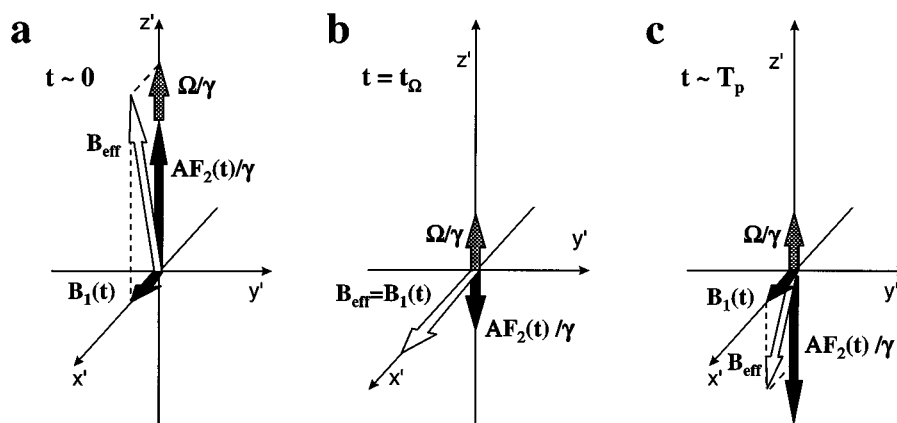


**Figure 4.** Effective field components in the FM frame at three different times during an AFP pulse for the case in which  $\Omega = \omega_0 - \omega_c > 0$ . (a) and (c) Far from resonance, the dominant contribution to  $B_{\text{eff}}$  is given by  $\gamma^{-1}\Delta\omega(t) = \gamma^{-1}[\Omega - AF_2(t)]$ . (b) When resonance is achieved at  $t_0$ ,  $[\Omega/\gamma]\hat{z}'$  and  $[AF_2(t_0)/\gamma]\hat{z}'$  cancel each other; thus, the effective field is solely determined by its transverse component,  $B_1(t_0)$ . The adiabatic condition at this time ( $|\gamma B_1(t_0)| \gg |d\alpha/dt|$ ) limits the ability to invert the isochromat  $\Omega$ .

smoothness of the transition at the extremities of the AM function can easily be tuned by adjusting the parameter  $n$ .

Although the pulses in Table 1 were designed for broadband applications (e.g.  $^{13}\text{C}$  decoupling), both  $\Delta\Omega$  and  $B_{1(99\%)}^0$  scale inversely with  $T_p$ . For example, when using the Gaussian OIA pulse with  $T_p = 10$  ms, approximately the same performance can be achieved for  $\Delta\Omega = 10$  kHz using  $\gamma B_{1(99\%)}^0 = 1.2$  kHz. Figure 5 shows this Gaussian OIA pulse, along with a simulation of its inversion profile produced with the latter parameters.

**Gradient-modulated offset-independent adiabaticity (GOIA)**

Here we continue the analysis considering the case of a time-dependent resonance offset resulting from a modulated magnetic field such as that produced by a gradient. For this case, the instantaneous frequency offset  $\Omega(t)$  of a given isochromat at position  $x$  is now defined as:

$$\Omega(t) = \gamma x G F_3(t) \tag{14}$$

**Table 1. Modulation functions and performance comparison<sup>a</sup> of OIA inversion pulses**

Pulse <sup>b</sup>	$F_1(\tau)$	$F_2(\tau)$	$\gamma B_{1(99\%)}^0$ (kHz)	$\gamma B_1^{\text{rms}}$ (kHz)	$\Omega$
Lorentz	$\frac{1}{1+\beta\tau^2}$	$\frac{\tau}{1+\beta\tau^2} + \frac{1}{\sqrt{\beta}} \tan^{-1}(\sqrt{\beta}\tau)$	11.49	3.25	15.08
HS	$\text{sech}(\beta\tau)$	$\frac{\tanh(\beta\tau)}{\tanh(\beta)}$	7.56	3.28	14.81
Gauss <sup>c</sup>	$\exp\left(-\frac{\beta^2\tau^2}{2}\right)$	$\frac{\text{erf}(\beta\tau)}{\text{erf}(\beta)}$	6.13	3.29	14.67
Hanning	$\frac{1+\cos(\pi\tau)}{2}$	$\tau + \frac{4}{3\pi} \sin(\pi\tau) \left[1 + \frac{1}{4} \cos(\pi\tau)\right]$	5.51	3.32	14.50
HSn <sup>c</sup> ( $n=8$ )	$\text{sech}(\beta\tau^n)$	$\int \text{sech}^2(\beta\tau^n) d\tau$	3.71	3.25	14.49
Sin40 <sup>d</sup> ( $n=40$ )	$1 - \left \sin^n\left(\frac{\pi\tau}{2}\right)\right $	$\tau - \int \sin^n\left(\frac{\pi\tau}{2}\right) \left(1 + \cos^2\left(\frac{\pi\tau}{2}\right)\right) d\tau$	3.61	3.29	14.20
Chirp	C (constant)	$\tau$	3.38	3.38	11.24

<sup>a</sup> All performance factors ( $B_{1(99\%)}^0$ ,  $B_1^{\text{rms}}$  and  $\Omega$ ) were determined from simulations using  $T_p = 2$  ms and  $A = 25$  kHz ( $\Delta\Omega = 50$  kHz).

<sup>b</sup> The parameter  $\beta$  was chosen to set the minimum value of  $F_1(\tau)$  equal to 0.01.

<sup>c</sup> These FM driving functions must be obtained by numerical integration of  $F_1(\tau)^2$ ,  $\tau = 2t/T_p - 1$ ,  $|\tau| \leq 1$  for  $0 \leq t \leq T_p$ .

<sup>d</sup> The second term of the FM function is more significant for lower  $n$  values and can be obtained in closed form, although the numerical integration of  $F_1(\tau)^2$  is simpler to perform.

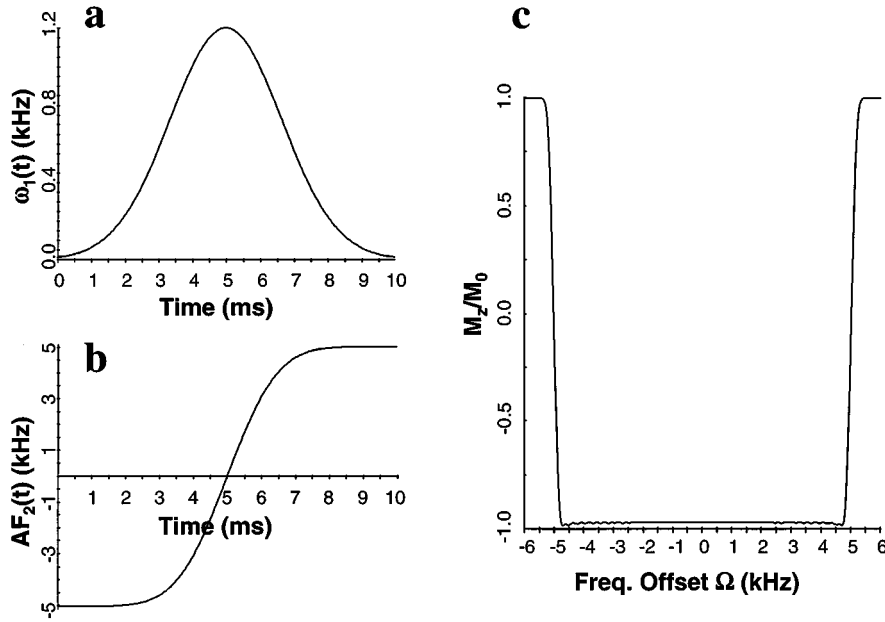


Figure 5. (a) AM and (b) FM functions of the Gaussian OIA pulse with  $T_p=10$  ms and  $A=5$  kHz, and (c) its inversion profile obtained from the numerical solution of the Bloch equations.

where  $G$  is the amplitude of the gradient and the driving function  $F_3(t)$ , like the other modulation functions, is normalized to 1. The time dependent gradient affects the response of the magnetization in two different ways. Both the Larmor frequency at a given position  $x$  and the spectral width of a slab of magnetization with thickness  $\delta x$  become functions of time. To account for this new variability, the concept of frequency sweep as used in the previous section must now be redefined. The *effective range* of the frequency sweep over  $\delta x$  and the respective sweep rate are based on the longitudinal ( $\hat{z}'$ ) component of the effective field written as

$$\Delta\omega(t)=[\Omega(t)-AF_2(t)]\hat{z}'=[\gamma\chi GF_3(t)-AF_2(t)]\hat{z}' \quad (15)$$

Previous attempts to enhance pulse performance using modulated gradients have been relatively successful, partially due to the robustness of adiabatic pulses. For example, Conolly *et al.*<sup>45</sup> developed a time distortion method similar to the one proposed by Baum *et al.*,<sup>32</sup> which in some cases can preserve the trajectory of  $\mathbf{B}_{\text{eff}}(t)$ . More recently, Ordidge *et al.*<sup>52</sup> devised a similar approach with FOCI pulses, where the  $\mathbf{B}_{\text{eff}}(t)$  trajectory was preserved by multiplying both its longitudinal and transverse components by the same weighting function  $W(t)$ . Both of these methods allow the generation of slice selective AFP pulses that require less RF power than the parent pulses for a specified bandwidth. However, these previous approaches were concerned with the *trajectory* of  $\mathbf{B}_{\text{eff}}(t)$  for the isochromat at  $\Omega=0$ , not its *power distribution* among distinct isochromats contained in the requested bandwidth. Consider, for example, an experiment where a FOCI pulse is applied with different values of  $B_1^0$ . As  $B_1^0$  increases, the borders of the magnetization profile become inverted sooner than the central region, which is a clear indication that the final result can be achieved with less RF energy. This phenomenon occurs because the FOCI amplitude modulation function is inadequate for the rate of sweep determined by its frequency and gradient modulation functions. In the analysis that follows we provide an analytical means to relate these functions based on the concept of offset independent adiabaticity.

The adiabatic condition  $K(\Omega, t)$  is now defined as:

$$K(\Omega, t) = \left| \frac{\gamma B_{\text{eff}}^{\Omega}(t)}{\dot{\alpha}} \right| = \frac{A^2}{\gamma B_1^0} \frac{[(\gamma B_1^0 F_1(t)/A)^2 + [F_2(t) - gF_3(t)]^2]^{3/2}}{|(F_2(t) - gF_3(t))\dot{F}_1(t) - F_1(t)[\dot{F}_2(t) - g\dot{F}_3(t)]|} \gg 1 \quad (16)$$

where  $g = \gamma\chi G/A$ . Once again we analyze the adiabatic condition (eq. (16)) at its most critical time, when the effective field is crossing the transverse plane ( $x'y'$ ). For all specific times  $t=t_\Omega$  when the isochromat at  $\Omega(t_\Omega)$  is on resonance, eq. [16] simplifies and  $K(\Omega, t)$  can be calculated from:

$$K(t_\Omega) = \frac{(\gamma B_1^0 F_1(t_\Omega))^2}{A[F_2(t_\Omega) - gF_3(t_\Omega)]} \gg 1 \quad (17)$$

The coordinate along the gradient direction is given by:

$$x(t_\Omega) = \frac{AF_2(t_\Omega)}{\gamma GF_3(t_\Omega)} \quad (18)$$

To achieve an effective sweep over spatially dispersed isochromats, eq. (18) demands that  $F_3(t)$  is not proportional to  $F_2(t)$ . The theoretical development for the case in which these functions are proportional to each other, as in GMAX<sup>43,56</sup> and BISS-8,<sup>16</sup> will be addressed in forthcoming work.

Upon substituting  $g$  and  $x(t_\Omega)$  into Eq. (17), the new identity is

$$K(t_\Omega)A \left[ \dot{F}_2(t_\Omega) - \frac{F_2(t_\Omega)\dot{F}_3(t_\Omega)}{F_3(t_\Omega)} \right] = (\gamma B_1^0 F_1(t_\Omega))^2 \quad (19)$$

The easiest way to generate OIA modulation functions from eq. (19) is to calculate  $F_1(t)$  given  $F_2(t)$  and  $F_3(t)$ . This direct approach, however, is not satisfactory since the resultant shape of  $B_1(t)$  can have undesirable properties, such as high

peak power. Figure 6 shows the AM function of a pulse obtained using this OIA approach based on the  $F_2(t)$  and  $F_3(t)$  functions of FOCI. The new pulse requires less area under the  $B_1(t)$  function, and thus lower RF energy, than the original FOCI pulse, while the inversion profile remains almost unchanged. However, its AM shape is still far from the desirable plateau needed to reduce RF peak power.

Alternatively, a reverse GOIA approach supplies  $F_1(t)$  and  $F_3(t)$ , and  $F_2(t)$  is obtained by solving the differential equation given by eq. (19) with initial condition  $F_2(T_p/2) = 0$ . An important point to be noticed here is that the shape of the solution is no longer independent of the magnitude of  $K$ , as it was in the previous section. Now  $K$  must be adjusted in order to allow the frequency sweep given by  $F_2(t)$  to fall in the interval  $[-A, A]$ .

To demonstrate the efficiency of the latter method, we start with the AM driving function ( $F_1(t)$ ) of an HS4 pulse. This choice is based on the ability of HS $n$  pulses (for  $n > 2$ ) to perform inversions with significantly reduced peak power.<sup>34</sup> Additionally, with  $n=4$  the AM shape of the pulse resembles that of a FOCI pulse (C-shaped<sup>52</sup>) of the same duration [see Fig. 7(a)]. For the time dependent gradient of GOIA, a function based on an HS2 AM shape,

$$F_3(t) = 1.0 - 0.9 \operatorname{sech} \left[ \beta \left( \frac{2t}{T_p} - 1 \right)^2 \right] \quad (20)$$

was chosen because of its smoothness and continuity of its derivatives. Other functions could be used, provided that higher gradient intensity is maintained at the times when the pulse is building the borders of the inversion profile and that lower gradient intensity occurs during the central region of the pulse, as shown in Fig. 7(c). Of course, experimental requirements and hardware limitations (e.g. gradient slew rate) may restrict the choices for the  $F_3(t)$  function. With the present choice of  $F_1(t)$  and  $F_3(t)$  functions, eq. (19) was used to calculate the driving function for the frequency modulation ( $F_2(t)$ ) shown in Fig. 7(b). By comparing  $B_1(t)$  functions [Fig. 7(a)], it can be seen that the GOIA pulse uses considerably less peak power (approximately half) to perform essentially with the same transformation as a FOCI

pulse with the same duration and bandwidth. As can be seen from Fig. 7(c), the GOIA pulse also reduces demands on gradient slew rate. To allow a performance comparison between GOIA and FOCI pulses, Figs 7(d) and 7(e) show plots of the power spectral density (PSD) and inversion profile ( $M_z/M_0$ ) for a GOIA pulse based on HS4 and a FOCI pulse of the same duration. Table 2 compares the  $B_1$  intensity ( $B_1^{0(99\%)}$ ) and peak and average power required by these pulses. For reference, these performance parameters are normalized to those of a square pulse of the same duration although its spectral composition is obviously different.

The ability of the pulses to distribute RF energy uniformly over the requested range of isochromats is apparent from Fig. 8 which shows  $M_z/M_0$  profiles as a function of  $\Omega$  and  $\omega_1$  intensity. As the  $\omega_1$  amplitude increases, the FOCI pulse inverts the isochromats at the borders earlier than the central portion of the profile [Fig. 8(a)]. With the GOIA pulse, a relatively uniform response is obtained for all  $\omega_1$  amplitudes [Fig. 8(b)].

### Practical aspects on the use of adiabatic pulses

The previous sections represent an attempt to explain the response of a spin system to adiabatic pulses and to propose methods to generate their modulation functions. Here we consider some practical aspects regarding experimentations of adiabatic pulses.

- When properly designed, adiabatic pulses do not necessarily deliver more RF power than conventional pulses. The common misconception that adiabatic pulses require high RF power may arise in part from the fact that certain adiabatic pulses allow much wider bandwidths than conventional pulses of the same duration. With OIA inversion pulses, the amount of power delivered per unit spectral width (or power spectral density, PSD) needs to be no greater than that required by conventional pulses in order to perform the same transformation on the spin system.<sup>34</sup> Since the energy of OIA pulses is distributed incrementally in time, the peak power can be even lower than that required by conventional pulses. Hence, these

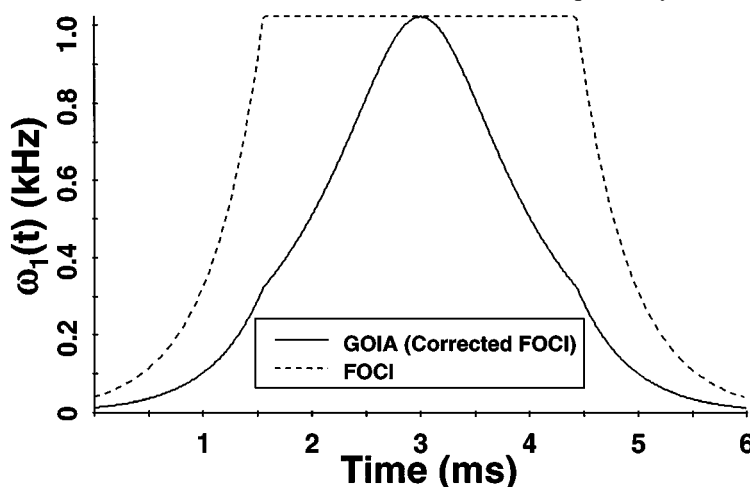
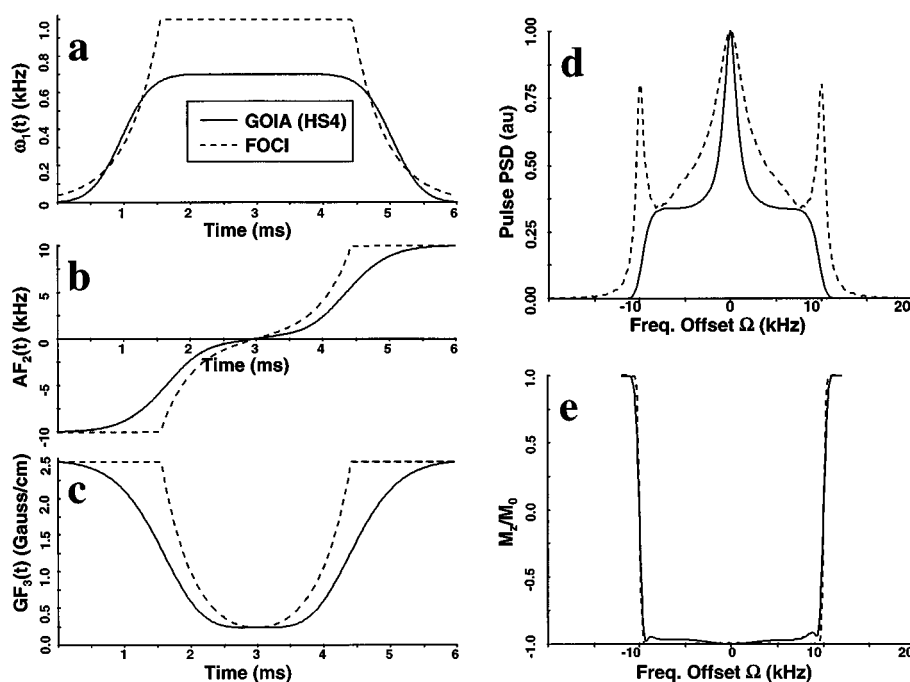


Figure 6. Amplitude modulation functions for FOCI (C-shaped) and a GOIA pulse. The solid line represents the AM function generated according to the direct GOIA method, starting with the FM and gradient modulation functions of the FOCI pulse. The inversion profile produced by this GOIA pulse is comparable to that of the original FOCI pulse using approximately the same  $B_1$  amplitude, but the GOIA pulse clearly delivers less RF energy.



**Figure 7.** Modulation functions for GOIA and FOCI (C-shaped) pulses and their performance profiles. The GOIA driving functions,  $F_1(t)$  for  $\omega_1(t)$  (a) and  $F_3(t)$  for gradient modulation (c) were supplied to calculate  $F_2(t)$  for the frequency modulation (b). From the AM function (a) and the simulated inversion profile (e), it can be seen that the GOIA pulse (solid line) uses considerably less peak power (approximately 50%) to perform essentially the same transformation as a FOCI pulse (dashed line) with same duration and bandwidth. To allow a comparison, plots of PSD (d) and inversion profile (e) are shown.

adiabatic pulses can be used generously in experiments formerly designed to accomplish the same tasks with conventional pulses provided that care is taken to avoid wastefully exceeding the threshold  $B_1$  intensity needed to accomplish the desired transformation.

- The ability to modulate the pulse frequency is not a feature of some NMR spectrometers. Most often, adiabatic pulses are implemented with phase instead of frequency modulation since digital phase shifters with high resolution ( $<1^\circ$ ) are commonly available. The phase modulation template ( $\Phi(t)$ ) to be accessed by the spectrometer can be obtained from the integral of the frequency modulation function ( $FM(t)$ ). The relationship between phase and frequency functions come from the oscillatory part of the complex pulse  $P(t)$  written as:

$$P(t) = AM(t) \cdot e^{i\Phi(t)} \quad (21)$$

where,

$$\Phi(t) = 2\pi \int FM(t) dt \quad (22)$$

and  $AM(t)$  is the amplitude modulation function.

- The frequency modulation amplitude  $A$  (see eq. (9)) determines the minimum sampling rate to obtain the pulse in digitized form. To demonstrate this fact, we introduce the unitless factor  $R = 2AT_p$ , which specifies the ratio between the total adiabatic pulse bandwidth ( $\Delta\Omega = 2A$ ) in hertz and the bandwidth of a conventional pulse of same duration (roughly given by  $1/T_p$ ). To avoid aliasing when defining the digital version of the pulse, the Nyquist theorem must be satisfied, and here it takes the form of the inequality:

$$\Delta f = \frac{1}{\delta t} \geq 2A \quad (23)$$

where  $\delta t = T_p/N$  is the duration of the sampling interval (dwell time), for which all modulation functions are piecewise constant, and  $N$  is the number of time samples. Therefore,  $\Delta f$  is the maximum overall bandwidth of the digitized pulse, and it follows from eq. (23) that:

$$N \geq 2AT_p (=R) \quad (24)$$

**Table 2.** Modulation functions and performance comparison of GOIA and FOCI inversion pulses<sup>a</sup>

Pulse	$F_1(\tau)$	$F_2(\tau)$	$F_3(\tau)$	$\gamma B_1^2$ (99%) (kHz)	Average power (au)	Peak power (au)
GOIA (HS4)	$\text{sech}(\beta\tau^4)$	$\frac{dF_2}{d\tau} - \frac{F_2}{F_3} \frac{dF_3}{d\tau} = \frac{F_1^2}{K}$	$1.0 - 0.9 \text{ sech}(\beta\tau^2)$	0.7	0.30	0.49
FOCI <sup>b</sup>	$\text{sech}(\beta\tau) \cdot F_3(\tau)$	$\tanh(\beta\tau)$	$\frac{\overline{\Pi}_{\tau_c}(\tau) \cosh(\beta\tau) + \underline{\Pi}_{\tau_c}(\tau) \cosh(\beta\tau_c)}{\underline{\Pi}_{\tau_c}(\tau) \cosh(\beta\tau)}$	1.0	0.56	1.0
Square	$C$ (Constant)	—	—	1.0	1.0	1.0

<sup>a</sup> Defined with  $T_p = 6$  ms ( $\tau = 2t/T_p - 1$ ,  $|\tau| \leq 1$  for  $0 \leq t \leq T_p$ ) and  $A = 10$  kHz ( $\Delta\Omega = 20$  kHz).

<sup>b</sup>  $F_3(\tau)$  is based on the Heaviside function,  $H(\tau)$ , and one of the roots ( $\tau_c$ ) of the equation  $\text{sech}(\beta\tau) = 0.1$  and is given by  $\overline{\Pi}_{\tau_c}(\tau) = H(\tau + \tau_c) - H(\tau - \tau_c)$  and  $\underline{\Pi}_{\tau_c}(\tau) = 1 - \overline{\Pi}_{\tau_c}(\tau)$ .

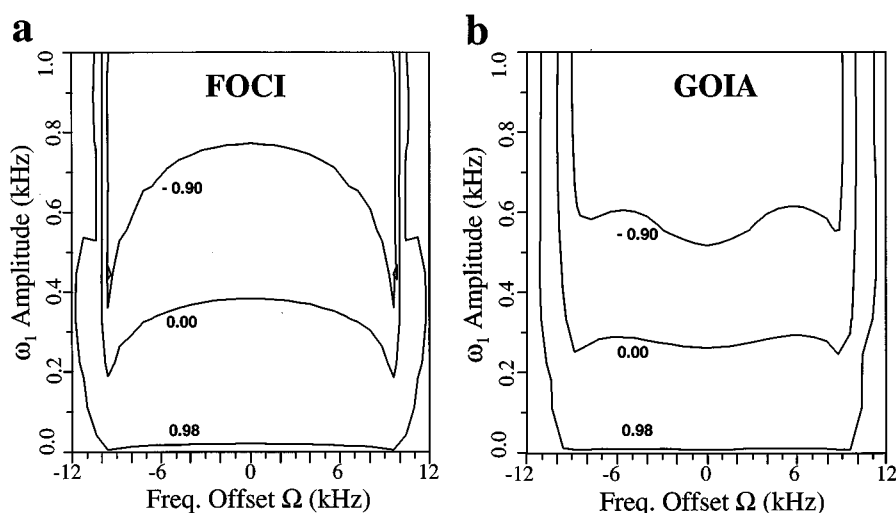


**Figure 8.** Contour plots of  $M_z/M_0$  vs  $\omega_1$  intensities and frequency offsets  $\Omega$  for (a) FOCI and (b) GOIA pulses with 20 kHz bandwidth and  $T_p=6$  ms. The maximum value in the  $\omega_1$  scale was chosen based on the minimum  $B_1$  intensity necessary for FOCI pulses to perform 99% inversion of the magnetization at  $\Omega=0$ . Evidence that the FOCI pulse performs complete inversion of the isochromats at the borders earlier than in the central portion of the profile is shown in (a). A relatively uniform response is obtained with the GOIA pulse for a wide range of  $B_1$  intensities as shown in (b).

must be satisfied. In other words, the number of digitized pulse samples must be at least equal to the numerical value of  $R$ . This requirement also applies to more complex adiabatic pulses such as BIR-1 and BIR-4.

## CONCLUDING REMARKS

In this review, adiabatic pulses were analyzed using a classical description suitable for isolated spins. For more complex spin interactions such as scalar or dipolar coupling, it will be necessary to invoke quantum mechanics formalism to obtain accurate descriptions of the effects of

adiabatic pulses on the spin systems.<sup>57,58</sup> Likewise, our optimizations of modulation functions were guided by the adiabatic condition, but other approaches, such as recursive expansion<sup>10,15</sup> and computer optimizations,<sup>59</sup> may yield further improvements. Finally, for the sake of brevity, it was not possible to consider all the many different types of adiabatic pulses that have been reported and their potential uses. Instead, we chose to focus on general principles and to limit our discussion to some of the more common pulses in use today.

## Acknowledgements

This work was supported by NIH Grants RR08079 and CA64338 and the Brazilian agency FAPESP.

## REFERENCES

- Purcell, E. M., Torrey, H. C. and Pound, R. V. Resonance absorption by nuclear magnetic moments in a solid. *Phys. Rev.* **69**, 37 (1946).
- Bloch, F., Hansen, W. W. and Packard, M. Nuclear induction. *Phys. Rev.* **69**, 127 (1946).
- Ernst, R. R. and Anderson, W. A. Application of Fourier transformation spectroscopy to magnetic resonance. *Rev. Sci. Instrum.* **137**, 93–101 (1966).
- Starcuk, Z., Bartusek, K. and Starcuk, Z. Heteronuclear broadband spin-flip decoupling with adiabatic pulses. *J. Magn. Reson. A* **107**, 24–31 (1994).
- Bendall, M. R. Broadband and narrowband spin decoupling using adiabatic spin flips. *J. Magn. Reson. A* **112**, 126–129 (1995).
- Kupce, E. and Freeman, R. Adiabatic pulses for wideband inversion and broadband decoupling. *J. Magn. Reson. A* **115**, 273–276 (1995).
- Fu, R. and Bodenhausen, G. Ultra-broadband decoupling. *J. Magn. Reson. A* **117**, 324–325 (1995).
- Hwang, T.-L., Garwood, M., Tannús, A. and van Zijl, P. C. M. Reduction of sideband intensities in adiabatic decoupling using modulation generated through adiabatic R-variation (MGAR). *J. Magn. Reson. A* **121**, 221–226 (1996).
- Levitt, M. H. and Freeman, R. NMR population inversion using a composite pulse. *J. Magn. Reson.* **33**, 473–476 (1979).
- Levitt, M. H. and Ernst, R. R. Composite pulses constructed by a recursive expansion procedure. *J. Magn. Reson.* **55**, 247 (1983).
- Ugurbil, K., Garwood, M. and Bendall, M. R. Amplitude and frequency modulated pulses to achieve 90° plane rotations with inhomogeneous  $B_1$  fields. *J. Magn. Reson.* **72**, 177–185 (1987).
- Bendall, R. M., Ugurbil, K., Garwood, M. and Pegg, D. T. Adiabatic refocusing pulse which compensates for variable RF power and off-resonance effects. *Magn. Reson. Med.* **4**, 493–499 (1987).
- Conolly, S., Nishimura, D. and Macovski, A. A selective adiabatic spin-echo pulse. *J. Magn. Reson.* **83**, 324–334 (1989).
- Staewen, R. S., Johnson, A. J., Ross, B. D., Parrish, T., Merkle, H. and Garwood, M. 3-D FLASH imaging using a single surface coil and a new adiabatic pulse, BIR-4. *Invest. Radiol.* **25**, 559–567 (1990).
- Garwood, M. and Ke, Y. Symmetric pulses to induce arbitrary flip angles with compensation for RF inhomogeneity and resonance offsets. *J. Magn. Reson.* **94**, 511–525 (1991).
- de Graaf, R. A., Nicolay, K. and Garwood, M. Single-shot,  $B_1$ -insensitive slice selection with a gradient-modulated adiabatic pulse, BISS-8. *Magn. Reson. Med.* **35**, 652–657 (1966).

17. Hwang, T.-L., van Zijl, P. C. M. and Garwood, M. Broadband adiabatic refocusing without phase distortion. *J. Magn. Reson.* **24**, 250–254 (1997).
18. Norris, D. G. and Haase, A. Variable excitation angle AFP pulses. *Magn. Reson. Med.* **9**, 435 (1989).
19. Abragam, A. *The Principles of Nuclear Magnetism*. Clarendon Press, 1978.
20. Solomon, I. Rotary spin echoes. *Phys. Rev. Lett.* **2**, 301–305 (1959).
21. Ross, B. D., Merkle, H., Hendrich, K., Staewen, R. S. and Garwood, M. Spatially localized *in vivo*  $^1\text{H}$  magnetic resonance spectroscopy of an intracerebral rat glioma. *Magn. Reson. Med.* **23**, 96–108 (1992).
22. Schupp, D. G., Merkle, H., Ellermann, J. M., Ke, Y. and Garwood, M. Localized detection of glioma glycolysis using edited  $^1\text{H}$  MRS. *Magn. Reson. Med.* **30**, 18–27 (1993).
23. Inglis, B. A., Sales, K. D. and Williams, S. C. R. BIRIANI, a new composite adiabatic pulse for water-suppressed proton NMR spectroscopy. *J. Magn. Reson. B* **105**, 61–66 (1994).
24. de Graaf, R. A., Luo, Y., Terpstra, M., Merkle, H. and Garwood, M. A new localization method using an adiabatic pulse, BIR-4. *J. Magn. Reson. B* **106**, 245–252 (1995).
25. Garwood, M. and Merkle, H. Heteronuclear spectral editing with adiabatic pulses. *J. Magn. Reson.* **94**, 180–185 (1991).
26. de Graaf, R. A., Luo, Y., Terpstra, M. and Garwood, M. Spectral editing with adiabatic pulses. *J. Magn. Reson. B* **109**, 184–193 (1995).
27. Garwood, M., Nease, B., Ke, Y., de Graaf, R. A. and Merkle, H. Simultaneous compensation for  $B_1$  inhomogeneity and resonance offsets by a multiple-quantum NMR sequence using adiabatic pulses. *J. Magn. Reson. A* **112**, 272–274 (1995).
28. Merkle, J. Wei, H., Garwood, M. and Ugurbil, K.  $B_1$ -Insensitive heteronuclear adiabatic polarization transfer for signal enhancement. *J. Magn. Reson.* **99**, 480–494 (1992).
29. Kim, S.-G. and Garwood, M. Double DEPT using adiabatic pulses. Indirect heteronuclear  $T_1$  measurement with  $B_1$  insensitivity. *J. Magn. Reson.* **99**, 660–667 (1992).
30. van Zijl, P. C. M., Hwang, T.-L., O'Neil Johnson, M. and Garwood, M. Optimized excitation and automation for high-resolution NMR using  $B_1$ -insensitive rotation pulses. *J. Am. Chem. Soc.* **118**, 5510–5511 (1996).
31. Silver, M. S., Joseph, R. I. and Hoult, D. I. Highly selective  $\pi/2$  and  $\pi$  pulse generation. *J. Magn. Reson.* **59**, 347–351 (1984).
32. Baum, J., Tycko, R. and Pines, A. Broadband and adiabatic inversion of a two-level system by phase-modulated pulses. *Phys. Rev. A* **32**, 3435 (1985).
33. Kupce, E. and Freeman, R. Optimized adiabatic pulses for wideband spin inversion. *J. Magn. Reson. A* **118**, 229–303 (1996).
34. Tannús, A. and Garwood, M. Improved performance of frequency-swept pulses using offset-independent adiabaticity. *J. Magn. Reson. A* **120**, 133–137 (1996).
35. Dunant, J. J. and Delayre, J., US Patent 3,975,765 (1976).
36. Baum, J., Tycko, R. and Pines, A. Broadband population inversion by phase modulated pulses. *J. Chem. Phys.* **79**, 4643–4647 (1983).
37. Hardy, C. J., Edelstein, W. A. and Vatis, D. Efficient adiabatic fast passage for NMR population inversion in the presence of radiofrequency field inhomogeneity and frequency offsets. *J. Magn. Reson.* **66**, 470–482 (1986).
38. Kunz, D. Use of frequency-modulated radiofrequency pulses in MR imaging experiments. *Magn. Reson. Med.* **3**, 377 (1986).
39. Bendall, M. R. and Pegg, D. T. Uniform sample excitation with surface coils for *in vivo* spectroscopy by adiabatic rapid half passage. *J. Magn. Reson.* **67**, 376–381 (1986).
40. Ugurbil, K., Garwood, M. and Rath, A. Optimization of modulation functions to improve insensitivity of adiabatic pulses to variations in  $B_1$  magnitude. *J. Magn. Reson.* **80**, 448–360 (1988).
41. Johnson, A. J., Ugurbil, K. and Garwood, M. Optimization of modulation functions to enhance  $B_1$  insensitivity and off-resonance performance of adiabatic pulses. *Society of Magnetic Resonance in Medicine, 8th Annual Meeting* (1989).
42. Wang, Z. Theory of selective excitation by scaled frequency-amplitude sweep. *J. Magn. Reson.* **81**, 617 (1989).
43. Johnson, A. J., Garwood, M. and Ugurbil, K. Slice selection with gradient-modulated adiabatic excitation despite the presence of large  $B_1$  inhomogeneities. *J. Magn. Reson.* **81**, 653–660 (1989).
44. Böhlen, J.-M., Rey, M. and Bodenhausen, G. Refocusing with chirped pulses for broadband excitation without phase dispersion. *J. Magn. Reson.* **84**, 191 (1989).
45. Conolly, S., Glover, G., Nishimura, D. and Macovski, A. A reduced power selective adiabatic spin-echo pulse sequence. *Magn. Reson. Med.* **18**, 28–38 (1991).
46. Ke, Y., Schupp, D. G. and Garwood, M. Adiabatic DANTE sequences for  $B_1$ -insensitive narrowband inversion. *J. Magn. Reson.* **96**, 663 (1992).
47. Skinner, T. E. and Robitaille, P. M. L. Adiabatic excitation using  $\sin^2$  amplitude and  $\cos^2$  frequency modulation functions. *J. Magn. Reson. A* **103**, 34 (1993).
48. Slotboom, J., Vogels, B. A. P. M., de Haan, J. G., Creyghton, J. H. N., Quack, G., Chamuleau, R. A. F. M. and Bové, W. M. J. Proton resonance spectroscopy study of the effects of L-ornithine-L-aspartate on the development of encephalopathy, using localization pulses with reduced specific absorption rate. *J. Magn. Reson. B* **105**, 147–156 (1994).
49. Kupce, E. and Freeman, R. Stretched adiabatic pulses for broadband spin inversion. *J. Magn. Reson. A* **117**, 246 (1995).
50. de Graaf, R. A., Luo, Y., Garwood, M. and Nicolay, K.  $B_1$ -insensitive, single-shot localization and water suppression. *J. Magn. Reson. B* **113**, 35–45 (1996).
51. Rosenfeld, D., Panfil, S. L. and Zur, Y. Analytic solutions of the Bloch equation involving asymmetric amplitude and frequency modulations. *Phys. Rev. A* **54**, 2439–2443 (1996).
52. Ordidge, R. J., Wylezinska, M., Hugg, J. W., Butterworth, E. and Franconi, F. Frequency offset corrected inversion (FOCI) pulses for use in localized spectroscopy. *Magn. Reson. Med.* **36**, 562–566 (1996).
53. Shen, J. Use of amplitude and frequency transformations to generate adiabatic pulses of wide bandwidth and low RF power deposition. *J. Magn. Reson. Series B* **112**, 131–140 (1996).
54. Rosenfeld, D., Panfil, S. L. and Zur, Y. Design of adiabatic pulses for fat-suppression using analytic solutions of the Bloch equation. *Magn. Reson. Med.* **37**, 793–801 (1997).
55. Slichter, C. P. *Principles of Magnetic Resonance*, 3rd edn. Springer, New York, 1990.
56. Tannús, A., Garwood, M., Panepucci, H. and Bonagamba, T. J. Localized proton Spectroscopy with 3D-GMAX. 9th Society of Magnetic Resonance in Medicine, New York, NY (1990).
57. Hediger, S., Meier, B. H., Kurur, N. D., Bodenhausen, G. and Ernst, R. R. NMR cross polarization by adiabatic passage through the Hartmann–Hahn condition (APHH). *Chem. Phys. Lett.* **233**, 283–288 (1994).
58. Capuani, S. Luca, F. D., Marinelli, L. and Maraviglia, B. Coherence-transfer process by adiabatic pulses. *J. Magn. Reson. Series A* **121**, 1–7 (1996).
59. Poon, C. S. and Henkelman, R. M. Robust refocusing pulses of limited power. *J. Magn. Reson. A* **116**, 161–180 (1995).